Effect of Ti^{4+} substitution on structural, transport and magnetic properties of $La_{0.67}Sr_{0.33}Mn_{1-x}Ti_xO_3$

2008 J. Phys.: Condens. Matter 20 075203

(http://iopscience.iop.org/0953-8984/20/7/075203)

J. Phys.: Condens. Matter **20** (2008) 075203 (12pp) doi:10.1088/0953-8984/20/7/075203

Effect of Ti^{4+} substitution on structural, transport and magnetic properties of $La_{0.67}Sr_{0.33}Mn_{1-x}Ti_xO_3$

Vishwajeet Kulkarni[1], K R Priolkar[1,4], P R Sarode[1], Rajeev Rawat[2], Alok Banerjee[2] and S Emura[3]

[1] Department of Physics, Goa University, Taliegao Plateau, Goa 403 206, India
[2] UGC-DAE Centre for Scientific Research, University Campus, Khandwa Road, Indore 452 017, India
[3] Institute of Scientific and Industrial Research, Osaka University, Mihoga-oka 8-1, Ibaraki, Osaka 567-0047, Japan

E-mail: krp@unigoa.ac.in

Received 1 October 2007, in final form 20 December 2007
Published 25 January 2008
Online at stacks.iop.org/JPhysCM/20/075203

Abstract

$La_{0.67}Sr_{0.33}Mn_{1-x}Ti_xO_3$ ($0 \leqslant x \leqslant 0.20$) polycrystalline materials are prepared by employing lower annealing temperature compared to the temperatures reported for the materials of the same composition. The transport and magnetic properties of these materials are significantly different from those compounds prepared at higher annealing temperature. Samples with $x < 0.10$ show metal–insulator transition and those with $x \geqslant 0.10$ exhibit insulating behavior over the entire temperature range investigated. A gradual transition occurs from the ferromagnetic-metallic state to the ferromagnetic-insulator state with increasing Ti substitution. Lattice parameters and bond lengths of Mn and its near neighbors however do not change appreciably with the dopant content x in these materials. It is shown that Ti^{4+} doping in the low-temperature annealed samples is inhomogeneous, resulting in isolated Mn rich regions that are connected by a variable range hopping polaron.

(Some figures in this article are in colour only in the electronic version)

1. Introduction

Colossal magnetoresistive (CMR) manganites are among the most studied materials in condensed matter physics [1, 2]. Physical properties of manganites are very sensitive to the method of preparation, the type of symmetry of the unit cell, A- and B-site cations, size effects, concentration of the substitute, heterovalent substitution, non-stoichiometry etc. Most of the CMR properties are explained in terms of double-exchange (DE) and/or superexchange interactions, charge localization via Jahn–Teller distortion with polaron formation, phase separation and site disorder. Yet there is no agreement on the correct theoretical description of CMR properties, due to the complexities involved. Lately, there has been a greater focus on the effect of the synthesis procedures on CMR properties of these materials. It is well known that CMR materials exhibit significantly different properties when they are prepared with different synthesis procedures, starting from the same initial composition. Various defects like cation vacancies, oxygen non-stoichiometry and cation site disorder develop in the crystal structure due to the synthesis procedure and the environment used to prepare these materials. However, the effect of synthesis procedure on the microscopic as well as macroscopic properties of these materials is quite complex and needs to be investigated further to understand the physics involved.

Effect of oxygen non-stoichiometry on properties of CMR samples has also been studied in great detail [3–7]. For example, the defect chemistry of $LaMnO_{3\pm\delta}$ is unique [8]. For $LaMnO_{3+\delta}$, the structure is $GdFeO_3$ type for $0 \leqslant \delta < 0.10$ and rhombohedral for $0.10 \leqslant \delta < 0.3$ [9]. Although traditionally lanthanum manganite is

[4] Author to whom any correspondence should be addressed.

considered as an anion excess compound ($LaMnO_{3+\delta}$), detailed investigations employing high-resolution electron microscopy and other cognate techniques have revealed the presence of metal vacancies ($La_{1-\gamma}Mn_{1-\gamma}O_3$) instead of interstitial oxygen ions [10, 11]. $LaMnO_3$ perovskites have been shown to tolerate a considerable portion of vacancies in the A site (La site), giving rise to compositions of the type $La_{1-\delta}MnO_3$ with the charge compensated by formation of Mn^{4+} [12]. The Mn^{4+} content in lanthanum manganites can be varied by altering the firing temperature and atmosphere. Oxygen-rich samples exhibit a ferromagnetic-metallic to paramagnetic-insulating transition due to the holes doped by cation vacancies. However, in deliberately prepared cation deficient material like $La_{1-x}MnO_{3+\delta}$, it has been argued that charge deficit due to vacancies on La sites would be preferably compensated by the formation of oxygen vacancies, rather than by oxidation of Mn^{3+} into Mn^{4+} ions. Recently, XRD and EXAFS studies [13] on vacancy doped $La_{1-x}MnO_{3+\delta}$ have shown that for La/Mn ratio below 0.9 there is phase segregation of $La_{0.9}MnO_3$ and parasitic Mn_3O_4, and T_C remains almost constant like that of $La_{0.9}MnO_3$.

The strontium doped $LaMnO_3$ series also exhibits both oxygen rich and oxygen deficient non-stoichiometry. Trukhanov *et al* [14, 15] have studied oxygen deficient $La_{1-x}Sr_xMnO_{3-\frac{x}{2}}$ compounds wherein ferromagnetic indirect superexchange is considered to be the cause of the magnetism. There are several reports [7, 11, 16, 17] on $La_{1-x}Sr_xMnO_{3+\delta}$ compounds, wherein cation vacancies in oxygen rich materials are considered to be equally distributed on A and B sites, given by $v = \frac{\delta}{(3+\delta)}$, whereas Tofield and Scott [3] and Mitchell *et al* [18] have shown that the A-site vacancies are predominant. Mizusaki *et al* have discussed various models for cation deficiency in $La_{1-x}A_xMnO_3$ [19], such as A-site cation substituting the B site and vice versa. However, there appears to be very little literature about B-site vacancies [20, 21] in these materials. Interestingly, Nakamura [22] has shown that a fraction of Mn ions enter A-site cation vacancies in $La_{1-\Delta}MnO_{3+\delta}$ and affect the properties of the material substantially.

In spite of the extensive work carried out on these materials, there is no clear understanding or consensus on the microscopic picture of the disorder caused by vacancies or dopant atoms in these materials. Moreover, the effect of dopant ions replacing heterovalent ions has not been studied so far. Such a disorder can have a tremendous effect on the properties of these materials and is expected to give some interesting results. Ti doped CMR manganites offer such an opportunity. The ionic radius of the Ti^{4+} ion is known to be in between those of Mn^{4+} and Mn^{3+} and there exists a distinct possibility that a fraction of Ti^{4+} ions substitute for Mn^{3+} ions, leading to oxygen non-stoichiometry (cation deficiency) or such inhomogeneities. The available literature on Ti substitution in manganites indicates that Ti^{4+} ions substitute the isovalent Mn^{4+} ions in these materials [24–33]. Recently, however, it has been shown that at high doping levels Ti^{4+} ions occupy Mn^{3+} sites in addition to Mn^{4+} sites [34]. The effect of lower-temperature annealing has also been studied recently [35]. It has been shown that by suitably modifying the preparation procedure Ti^{4+} ions can substitute Mn ions randomly in $La_{0.67}Sr_{0.33}Mn_{1-x}Ti_xO_3$, forming inhomogeneous short-range ordered ferromagnetic clusters. Here we report a detailed investigation of structural, magnetic, transport and spectroscopic properties of lower-temperature annealed $La_{0.67}Sr_{0.33}Mn_{1-x}Ti_xO_3$ ($0 \leqslant x \leqslant 0.2$) using techniques such as XRD, resistivity, AC and DC susceptibilities, XPS, Mn and La K-edge EXAFS and IR spectroscopy. Since the annealing temperature of these materials is substantially lower than that reported in [27, 29], we term these low-temperature annealed materials. For comparison, the $x = 0.10$ sample has been prepared at the same annealing temperature as in [27] and is referred to as the high-temperature annealed sample.

2. Experimental details

Polycrystalline samples of $La_{0.67}Sr_{0.33}Mn_{1-x}Ti_xO_3$ with x = 0.0, 0.03, 0.05, 0.10 and 0.20 were synthesized by the conventional solid-state reaction method. The powders of La_2O_3, $SrCO_3$, freshly prepared $MnCO_3$ and TiO_2 with proper stoichiometry were mixed, ground manually using an agate mortar and pestle and fired in air at 1000 °C for about 15 h and reground to calcine at 1100 °C for 20 h. Finally, they were pressed into pellets and sintered in air at 1200 °C for 20 h. The grinding period was about half an hour every time. The $x = 0.10$ sample was also prepared by firing the ingredients in stoichiometric proportions at 1000, 1200 °C and annealing at 1450 °C, which closely matches the conditions reported in [27, 29]. In this case however the intermediate grinding was done manually with an agate mortar and pestle for about 3 h.

The samples were characterized by x-ray powder diffraction recorded on a Siemens D5000 diffractometer at room temperature between $2\theta = 10°$ and 70° with a step 0.05°. For AC susceptibility measurements, the samples were cooled under zero magnetic field and measurements were carried out in the warming run under the applied field of 0.936 Oe and AC frequency 133.33 Hz from liquid nitrogen temperature to 310 K on an in-house AC susceptometer [36]. For the samples with $x = 0.00$ and 0.03, the susceptibility measurements were carried out up to 365 K and 330 K, respectively. The standard four-probe technique was used to measure the resistivity of the samples in the temperature interval 300–80 K. Magnetoresistance (MR) measurements were performed down to 30 K using the standard four-probe geometry in longitudinal magnetic fields up to 5 T using an Oxford Spectromag 10 T superconducting magnet. Infrared measurements were performed on a Shimadzu FTIR-8900 spectrophotometer at room temperature in transmission mode in the range of 350–1000 cm^{-1}. The samples were mixed with KBr in the ratio 1:100 by weight and pressed into pellets for IR measurements. XPS study was carried out in an ESCA-3 Mark II spectrometer (VG Scientific Ltd., England) employing Al Kα radiation (1486.6 eV) at a pass energy of 50 eV. The powder samples were made into pellets of 8 mm diameter and placed into a UHV chamber housing the analyzer at 10^{-9} Torr. Before the measurements were carried out, the samples were kept in the preparation chamber for 5 h for desorption of gases. Binding energies were measured with a precision of

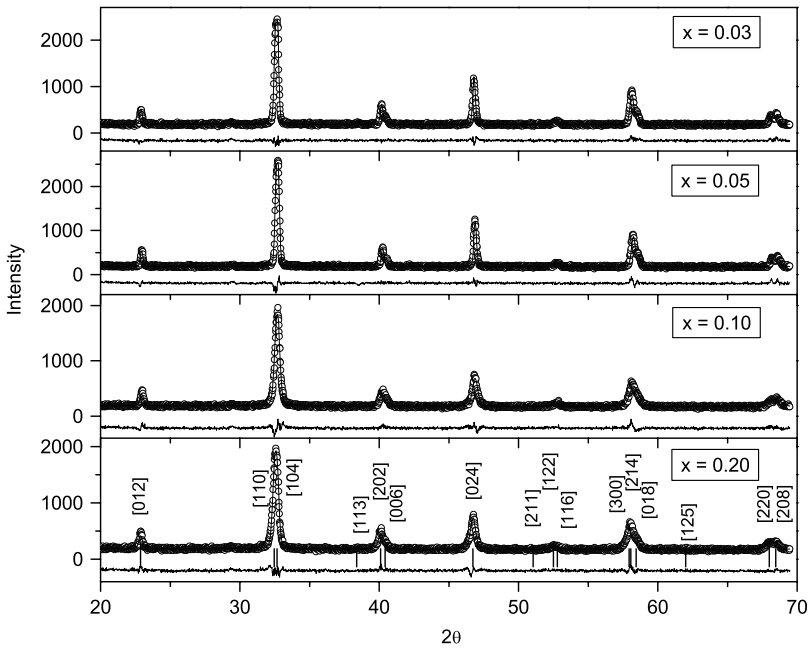

Figure 1. X-ray diffraction patterns (shown with circles) for low-temperature annealed $La_{0.67}Sr_{0.33}Mn_{1-x}Ti_xO_{3+\delta}$ ($0 \leqslant x \leqslant 0.20$) samples and their Rietveld fits (shown with a line). Vertical lines in the bottom panel indicate the Bragg reflection positions.

± 0.1 eV. The charging effect was taken care of with respect to the C(1s) peak of adventitious carbon at 285 eV. XAFS spectra at La and Mn K-edges were recorded using the BL01B1 XAFS beam-line at SPring-8. An Si(111) crystal served as the monochromator for Mn K-edge EXAFS and Si(311) for La K-edge EXAFS. For Mn K-edge measurements, fine powder of the sample was brushed onto Scotch tape. A number of layers of tape were stacked to obtain total absorption lengths $\mu x \approx 2.5$ (where x is the thickness of the sample). For La K-edge measurements, the absorbers were made by pressing the samples into pellets of 10 mm diameter with boron nitride as binder. The thickness (x) of the absorber was adjusted such that $\mu x \geqslant 1$. The pre-edge absorption was removed by fitting the data to a linear background and a simple cubic spline was used to simulate the embedded-atom absorption, μ_0, above the edge. The XAFS oscillations χ were obtained as a function of photoelectron wavevector $k = \sqrt{2m(E - E_0)/h^2}$. E_0 was estimated from the first inflection point of the main edge. XAFS oscillations, $\chi(k) = (\mu - \mu_0)/\Delta\mu$ (k—photoelectron wavenumber, μ_0—atomic absorption coefficient—and $\Delta\mu$—edge jump), were extracted following standard procedures. The FEFFIT program [37] was used to fit Fourier transformed (FT) $k\chi(k)$ data in r space to the theoretical spectra calculated using FEFF6.01 [38]. The Mn and La K-edge EXAFS data were analyzed in tandem, to improve the reliability of fits.

3. Results

3.1. X-ray diffraction

The x-ray diffraction patterns of $La_{0.67}Sr_{0.33}Mn_{1-x}Ti_xO_{3+\delta}$ ($0 \leqslant x \leqslant 0.20$) and the fits obtained from Rietveld refinement of the x-ray diffraction data are presented in figure 1. All the samples crystallize in a single phase rhombohedral structure (space group $R\bar{3}C$). Lattice parameters calculated for a hexagonal setting of the space group are found to be $a = 5.486$ Å and $c = 13.345$ Å for the pristine sample (table 1). These values closely match those reported earlier [27]. A monotonic increase in lattice parameters has been observed by Kallel *et al* [27] and Kim *et al* [29] for increasing doping content x in their Ti doped $La_{0.7}Sr_{0.3}MnO_3$ samples. They have ascribed the increase in lattice parameters to larger Ti^{4+} ions substituting smaller Mn^{4+} ions. In our samples, we observe non-systematic and relatively insignificant changes in the lattice parameters with the doping content x. Recently, Zhu *et al* [34] have reported that in thin films of $La_{0.67}Sr_{0.33}Mn_{1-x}Ti_xO_{3+\delta}$, the lattice parameters initially increase with doping content x for $x \leqslant 0.3$ and decrease for further doping. The decrease in the lattice parameters is said to be due to smaller Ti^{4+} ions substituting larger Mn^{3+} ions. The nearly constant lattice parameters observed in our samples could therefore be possible if Ti^{4+} ions substitute both larger Mn^{3+} and smaller Mn^{4+} ions at random.

Table 1. Doping content, excess oxygen, lattice parameters a and c, susceptibility, calculated spin-only susceptibility, and T_C for low-temperature annealed $La_{0.67}Sr_{0.33}Mn_{1-x}Ti_xO_{3+\delta}$. * implies VRH supported ferromagnetic transition around room temperature.

x	δ	a (Å)	c (Å)	χ_{exp} (μ_B/f.u. Oe)	$\chi_{spin\text{-}only}$ (μ_B/f.u. Oe)	T_C (K)
0	0.00	5.49(1)	13.35(1)	3.53	3.67	360
0.03	0.01	5.49(1)	13.36(1)	1.79	3.58	325
0.05	0.02	5.49(1)	13.34(1)	2.55	3.52	305
0.10	0.03	5.49(1)	13.34(1)	0.75	3.37	∼300*
0.20	0.05	5.50(1)	13.36(1)	0.76	3.07	∼300*

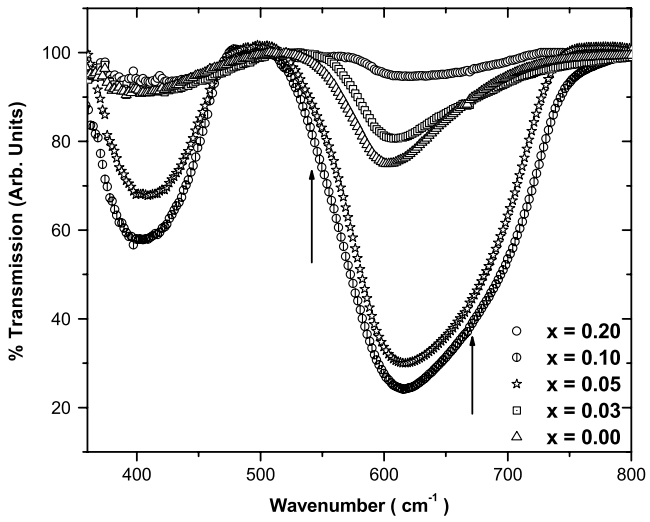

Figure 2. IR transmission spectra of low-temperature annealed $La_{0.67}Sr_{0.33}Mn_{1-x}Ti_xO_3$ ($0 \leqslant x \leqslant 0.20$). Arrows indicate Ti–O stretching modes.

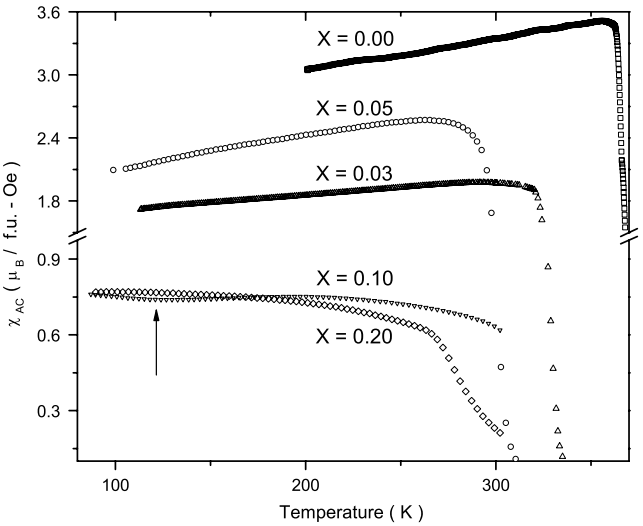

Figure 3. AC susceptibility–temperature plots of low-temperature annealed $La_{0.67}Sr_{0.33}Mn_{1-x}Ti_xO_{3+\delta}$ ($0 \leqslant x \leqslant 0.20$). The arrow indicates the second ferromagnetic transition in the $x = 0.10$ sample.

3.2. Infrared absorption studies

To investigate the valence of Ti ions, IR transmission spectra of the samples were recorded (figure 2). For the undoped sample, two broad absorption peaks are clearly seen between 350 and 500 cm^{-1} and 500–750 cm^{-1}, respectively. The first peak between 350 and 500 cm^{-1} is attributed to the Mn–O–Mn bending mode and the second to the Mn–O stretching mode of vibration [39, 40]. The widening of the stretching peak with doping content x may be induced due to the Mn–O and Ti–O stretching vibrations in Mn–O–Ti structure. Two additional shoulders at 670 and 540 cm^{-1} appear in heavily doped Ti samples. These frequencies match closely with TiO_2 absorption peaks [23], indicating that Ti is primarily in the tetravalent state. Recently temperature dependent IR absorption studies have been reported on some of these compounds [35].

3.3. Magnetic susceptibility

Plots of AC magnetic susceptibility as a function of temperature for $La_{0.67}Sr_{0.33}Mn_{1-x}Ti_xO_3$ ($0 \leqslant x \leqslant 0.20$) samples are presented in figure 3. For $0.0 \leqslant x \leqslant 0.05$, a sharp rise in AC susceptibility is seen, indicating a paramagnetic to ferromagnetic transition. The ferromagnetic ordering temperature (T_C) decreases with increasing doping content. T_C obtained for the parent compound is close to 360 K, which is as reported earlier [41], and it decreases to 325 and 305 K for $x = 0.03$ and 0.05, respectively (table 1). However, AC susceptibility of the $x = 0.05$ sample is greater than that of the $x = 0.03$ sample. Such anomalies have been reported earlier [42, 43]. Blasco *et al* [42] have attributed it to the magnetic inhomogeneity in their samples. In our case too, the anomaly may perhaps be due to the non-uniform distribution of magnetic $Mn^{3+/4+}$ ions in the sample. It is also possible that the Mn^{3+} content in the $x = 0.03$ sample is smaller than that in the $x = 0.05$ sample. Such a possibility does exist and can be seen in the error estimates of Mn^{3+} and Mn^{4+} contents in the two samples (table 3). For $x = 0.10$, AC susceptibility exhibits two distinct features close to 300 and 120 K, respectively. This sample has a ferromagnetic-like transition just above 300 K but the magnitude of the susceptibility per formula unit (f.u.) is very much less than the calculated spin-only moment value for a fully ordered sample (table 1). Susceptibility again shows a tendency to increase around 120 K. Such a behavior has been reported in $La_{1.4}Sr_{1.6}Mn_{2-y}Ti_yO_7$ [44]. For $x = 0.2$, a similar weak and broad magnetic transition is observed at about 300 K with the slope of the AC susceptibility–temperature curve being negative over the entire temperature range. It may be mentioned here that the calculated moment values shown in table 1 are with an assumption that Ti^{4+} ions substitute only Mn^{4+} ions.

To investigate the magnetic properties further, DC susceptibility measurements were carried out in the temperature range of 300–10 K in an applied field of 100 Oe on $0.00 \leqslant x \leqslant 0.20$ samples, using a Faraday balance. Similar measurements were also carried out on the high-temperature annealed $x = 0.10$ sample. The susceptibility of the high-temperature annealed sample with $x = 0.10$ shows a single ferromagnetic transition at temperature 220 K (figure 4(a)), whereas the corresponding low-temperature annealed sample shows two transition-like features at 300 K and 120 K, respectively (figure 4(b)). Susceptibility at saturation is substantially more for the high-temperature annealed sample compared to that of the corresponding low-temperature annealed sample. The weak susceptibility observed around 300 K in the low-temperature annealed sample is not visible in the high-temperature annealed sample.

In other Ti doped $La_{1-x}B_xMnO_3$ (B = Ca, Pb, Sr) compounds, in which Ti^{4+} ions are reported to substitute only Mn^{4+} ions, T_C continuously decreases as a function of dopant concentration x. This is due to the weakening of double-exchange interaction between Mn^{3+}–O–Mn^{4+} chains. In the

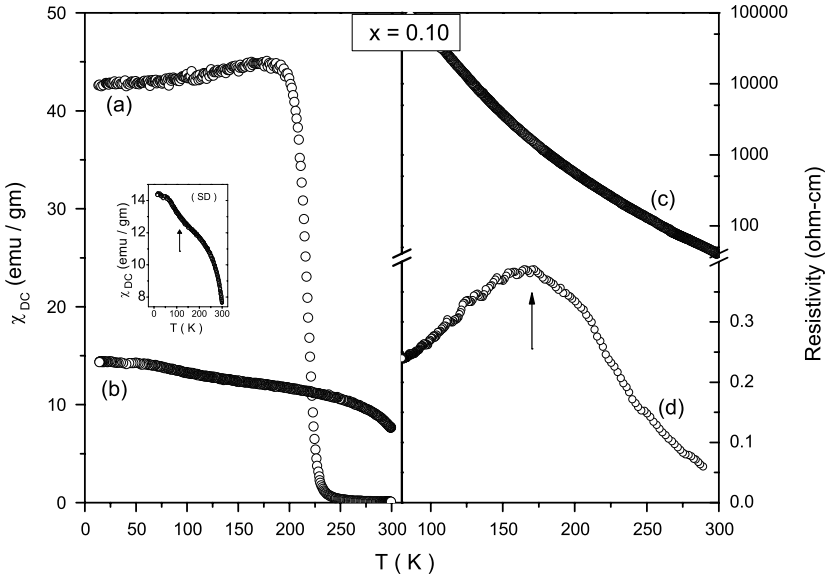

Figure 4. Temperature dependence of DC susceptibility for $La_{0.67}Sr_{0.33}Mn_{0.90}Ti_{0.10}O_{3+\delta}$ (a) high-temperature annealed and (b) low-temperature annealed samples and resistivity of (c) low-temperature annealed and (d) high-temperature annealed samples. The second ferromagnetic transition in the low-temperature annealed sample is indicated by an arrow in the inset.

present case, T_C initially decreases up to $x = 0.05$ and then remains at about 300 K for the further doping $0.10 \geqslant x \geqslant 0.20$.

Excess oxygen concentration or equivalently cation vacancies [45] in the samples and non-magnetic Ti ions isolate the regions of DE pairs from one another and result in lower susceptibility of the samples. Yet, higher T_C observed in the samples $x \geqslant 0.10$ could be possible if such isolated DE pairs are ferromagnetically linked with one another via a hopping polaron. Polaronic conduction could probably explain the higher T_C for $x \geqslant 0.10$ samples. In order to ascertain the exact mechanism responsible for the higher T_C for $x \geqslant 0.10$ samples, transport properties of this series have been studied.

3.4. Resistivity

The resistivity as a function of temperature is plotted in figure 5 for the Ti doped samples along with the parent compound $La_{0.67}Sr_{0.33}MnO_3$. The parent compound shows a metallic behavior in the entire temperature range studied, which augurs well with its metal–insulator (M–I) transition temperature of about 330 K [41]. At $x = 0.03$ and 0.05, M–I transition takes place at 270 K and 260 K, respectively. For $x \geqslant 0.10$, the low-temperature annealed sample exhibits insulating behavior throughout the temperature range studied while the high-temperature annealed sample ($x = 0.10$) shows the M–I transition at 180 K (figure 4(d)). Increase in resistivity with doping content x in the low-temperature annealed samples is mainly due to the weakening of the Mn^{3+}–O–Mn^{4+} DE bonds by interspersed Ti ions. At $x \geqslant 0.10$, the ferromagnetic double-exchange energy reduces to the extent that it does not become comparable to the thermal energy at any temperature down to 80 K so as to bring about the M–I transition. It is to be noted that the corresponding high-temperature annealed sample exhibits M–I transition.

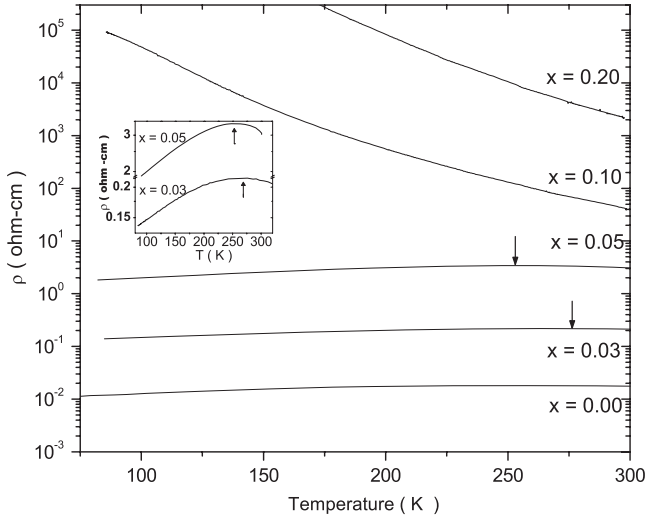

Figure 5. Resistivity versus temperature plots of low-temperature annealed $La_{0.67}Sr_{0.33}Mn_{1-x}Ti_xO_{3+\delta}$ ($0 \leqslant x \leqslant 0.20$). Arrows in the inset show the metal–insulator transition in $x = 0.03$ and 0.05 samples.

To study the transport mechanism of the charge carriers, generally three models are discussed for semiconductor-like behavior: the band-gap model [46], a nearest-neighbor hopping (NNH) model [47] for the transport of small polarons and a variable range hopping (VRH) model [48]. In the band-gap model, the resistivity of the sample is given by the Arrhenius law $\rho = \rho_0 \exp(E_\rho / k_B T)$. This equation could not be fitted to the resistivity curves of our low-temperature annealed samples, indicating that the activated transport across the band-gap does not occur in these samples in the temperature range studied. For the NNH model, the resistivity is given by $\rho = AT \exp(W_P / k_B T)$ with $W_P = E_P/(2 - t)$.

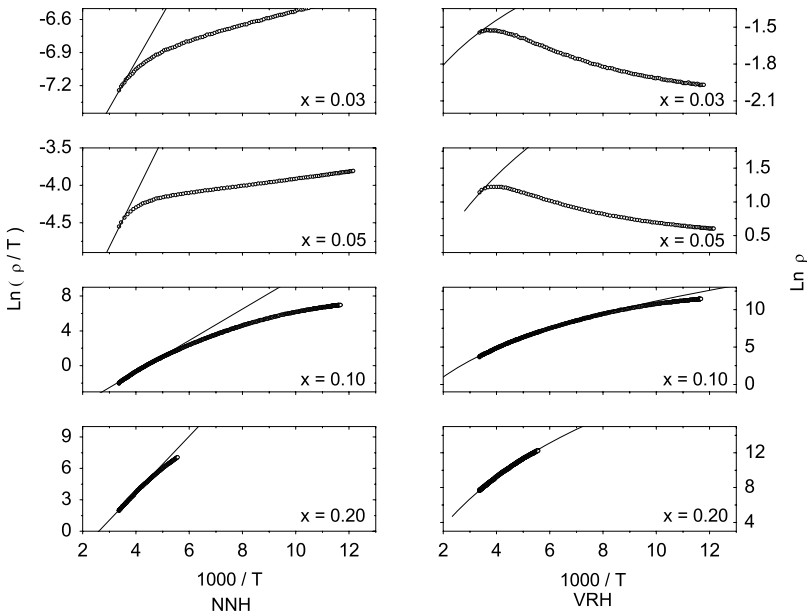

Figure 6. Nearest-neighbor and variable range hopping fits shown with $\ln \rho$ and $\ln(\rho/T)$ as a function of $(1000/T)$ for low-temperature annealed $La_{0.67}Sr_{0.33}Mn_{1-x}Ti_xO_{3+\delta}$ ($0.03 \leqslant x \leqslant 0.20$).

Table 2. Doping content and lower temperature limit down to which NNH or VRH fit is possible for low-temperature annealed $La_{0.67}Sr_{0.33}Mn_{1-x}Ti_xO_{3+\delta}$, higher limit being 300 K.

x	NNH (K)	VRH (K)
0.03	276	291
0.05	282	280
0.10	217	130
0.20	236	Entire range[a]

[a] Resistivity could not be measured below 180 K due to the high resistivity of the sample.

E_P denotes the polaron formation energy and t the electronic-transfer integral. In Mott's VRH model, the resistivity is expressed in the form of $\rho = \rho_{inf} \exp(T_0/T)^{1/4}$ [44]. Figure 6 shows that up to $x = 0.05$ the transport of the charge carriers in the insulating region can be explained by both NNH and VRH. For $x = 0.20$, resistivity can be fitted only by the VRH equation and for $x = 0.10$, resistivity deviates from VRH behavior below 130 K. For $x = 0.20$ resistivity could not be measured below 180 K due to its very high value. The details of the fitting ranges are presented in table 2. Further, it may be noted that for the $x = 0.10$ sample the deviation of resistivity from the VRH curve at 130 K matches closely with the second transition observed in susceptibility plots in figures 3 and 4(b). The weak ferromagnetic transition around 300 K could then be due to the interaction between Mn ions via a hopping polaron. Below 130 K the hopping energy weakens and Mn rich ferromagnetic regions get isolated. These isolated ferromagnetic regions then order, leading to the second ferromagnetic transition. In the sample with $x = 0.20$, perhaps the VRH mechanism extends to a still lower temperature and the second transition is therefore not distinctly observed.

Table 3. Percentage Mn^{4+} and Mn^{3+} contents in low-temperature annealed $La_{0.67}Sr_{0.33}Mn_{1-x}Ti_xO_{3+\delta}$ samples obtained from XPS data. Ti content was kept fixed to its nominal value. Figures in the bracket indicate the maximum estimated error.

Doping content (x)	Mn^{4+}	Mn^{3+}	Ti^{4+}
0.03	32.2(0.9)	64.8(0.9)	3
0.05	32.9(0.7)	64.1(0.7)	5
0.10	27.7(0.8)	62.3(0.8)	10
0.20	23.7(0.8)	56.3(0.8)	20

It is to be noted that the charge transport in the high-temperature annealed $x = 0.10$ sample clearly shows activated behavior across a band-gap. An exponential curve could be fitted to the resistivity–temperature plot of this sample between 228 K and room temperature. Thus the absence of M–I transition in the low-temperature annealed $x = 0.1$ sample can be understood to be due to inhomogeneous substitution of Ti^{4+} ions, whereas in the high-temperature annealed samples the decrease in the M–I transition temperature with increasing Ti doping level can be ascribed to the replacement of some of the Mn^{3+}–O–Mn^{4+} bonds by the Mn^{3+}–O–Ti^{4+} bonds. This could be either due to the grain boundary effect or the disorder in Ti doping at lower annealing temperatures. If grain boundaries are the cause of higher resistance, then the volume fraction sensitive properties like magnetization should not be affected [49]. However, it can be clearly seen that the behavior of magnetization for $x = 0.1$ of both high-temperature annealed and low-temperature annealed samples is different. Hence the grain boundary effect can be ruled out. A disorder in Ti substitution could create isolated Mn^{3+}–O–Mn^{4+} pairs connected through a polaron with a variable hopping range. This fact highlights the importance of VRH in transport and magnetic properties, and especially high T_C, in $x \geqslant 0.10$ low-temperature annealed samples.

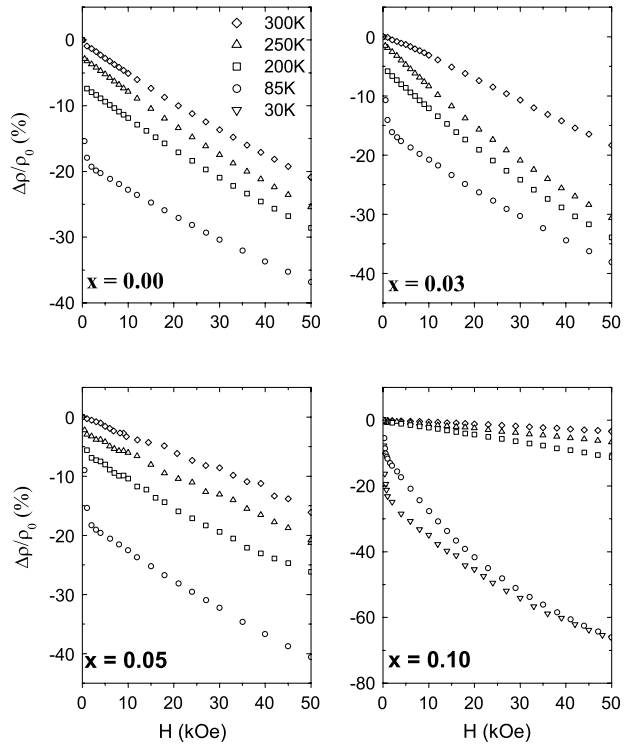

Figure 7. Magnetoresistance versus applied magnetic field plots of low-temperature annealed $La_{0.67}Sr_{0.33}Mn_{1-x}Ti_xO_{3+\delta}$ ($0 \leqslant x \leqslant 0.10$).

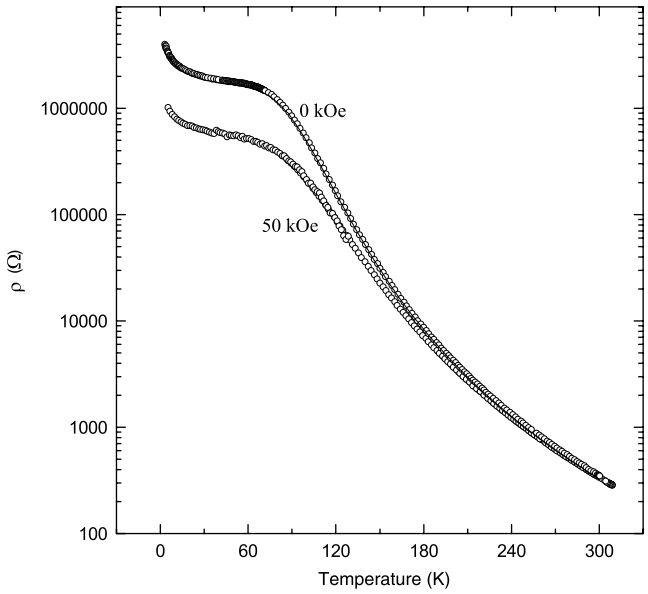

Figure 8. Resistivity under zero field and 5 T field for the low-temperature annealed $x = 0.10$ sample.

3.5. Magnetoresistance (MR)

Isothermal MR is negative for all the low-temperature annealed samples ($0.00 \geqslant x \geqslant 0.20$) (figure 7). For $x = 0.00$, MR shows H^2 dependence in all the isothermals, which is consistent with the ferromagnetic order of the sample. The magnetoresistance of $La_{0.7}Sr_{0.3}MnO_3$ has been reported [41] to be 45% at room temperature under the field of 6 T. The magnetoresistance observed for the parent sample $La_{0.67}Sr_{0.33}MnO_3$ in our series is 38% at room temperature and under the field of 5 T. The extrapolation of the isothermal MR to 6 T shows that the MR observed matches closely with that reported in [41]. Isothermal MR for samples with $x = 0.00$, 0.03 and 0.05 increases gradually at all the temperatures at which MR is recorded. However for $x = 0.10$, the isothermal MR is smaller than those of $x = 0.00$, 0.03 and 0.05 up to 210 K and increases substantially between temperatures 210 and 85 K. The sudden increase in MR points towards a ferromagnetic transition within this temperature range. It is clear from the susceptibility plots (figures 3 and 4(b)) that this sample has a second magnetic transition at about 120 K. The plot of resistivity in the presence of magnetic field ($H = 5$ T) also shows a deviation at about the same temperature from the zero-field resistivity curve (figure 8).

MR is shown to be much higher at the ferromagnetic transition temperature in the case of $La_{0.815}Sr_{0.185}MnO_3$ [17] and cation deficient $LaMnO_3$ [45]. In this case however, MR for the low-temperature annealed $x = 0.10$ sample is very small from 300 to 210 K in spite of a ferromagnetic transition at about 300 K. MR at 300 K is only of the order of 4% as compared to, 50% observed by Hébert *et al* [45] and around 45% to 66% for increasingly cation deficient samples studied by Bukowaski *et al* [17]. The low MR at 300 K further rules out the grain boundary effect as it would induce intergrain tunneling MR. Moreover, the sudden increase in MR between 200 and 80 K indicates that the ferromagnetic transition temperature lies somewhere within this range. These facts clearly indicate that ferromagnetic transition at room temperature observed in low-temperature annealed $x \geqslant 0.10$ samples is due to VRH transport of charge carriers that connects regions of DE pairs isolated from one another by non-magnetic Ti ions.

3.6. XPS Studies

From the above studies it is clear that in the low-temperature annealed samples doping of Ti^{4+} for Mn ions results in isolated Mn rich regions wherein DE is active. If this is indeed the case then the ratio of Mn^{3+} to Mn^{4+} should not increase exponentially due to depletion of Mn^{4+} by Ti^{4+}. To estimate Mn^{4+} and Mn^{3+} contents, x-ray photoelectron spectra of Mn 2p levels have been recorded for all the samples. Figures 9 and 10 show the Mn 2p x-ray photoelectron spectra of the samples in the range $0.0 \leqslant x \leqslant 0.20$. The Mn 2p spectra exhibit two main peaks around 642.5 and 654 eV. The two main peaks correspond to the spin–orbit split $2p_{\frac{3}{2}}$ and $2p_{\frac{1}{2}}$ levels, whereas the weak structure at around 24 eV from the main peak is the satellite of the $2p_{\frac{1}{2}}$ peak. The satellite of the $2p_{\frac{3}{2}}$ peak is not visible because it overlaps with the $2p_{\frac{1}{2}}$ peaks. The two main peak features were deconvoluted into those corresponding to $2p_{\frac{1}{2}}$ and $2p_{\frac{3}{2}}$ states of Mn^{3+} and Mn^{4+} ions and their satellites, with the help of a curve fitting Peakfit software program. The peaks for $2p_{\frac{3}{2}}$ ions are higher in binding energy than those for $2p_{\frac{1}{2}}$ states by about 11.6 eV. The Mn^{4+} and Mn^{3+} contents are calculated from areas under

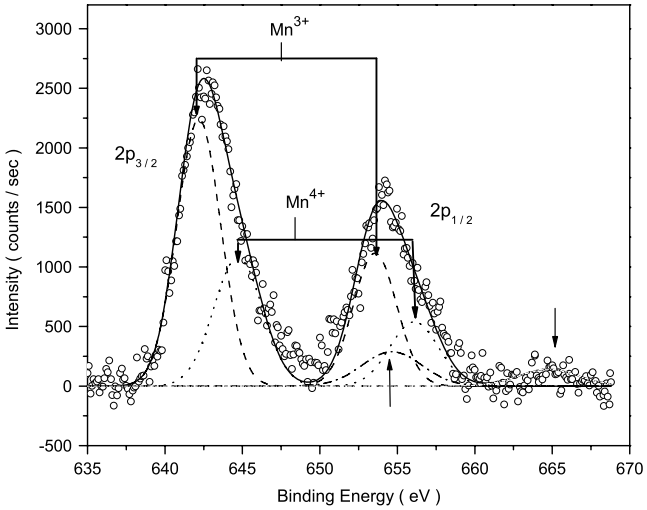

Figure 9. XPS spectrum (circles) of $La_{0.67}Sr_{0.33}MnO_3$ sample along with fitted curve (line). Discontinuous lines represent the deconvoluted $2p_{3/2}$ and $2p_{1/2}$ spectra corresponding to Mn^{3+} and Mn^{4+} ions. Arrows indicate the satellite peaks.

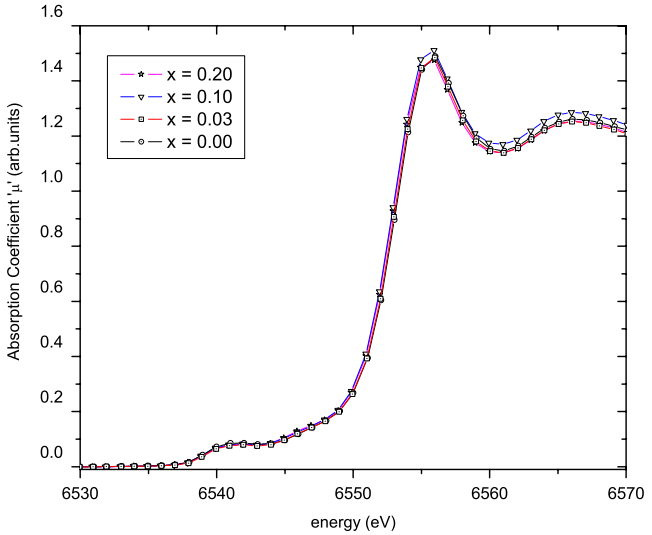

Figure 11. Normalized XANES spectra of low-temperature annealed $La_{0.67}Sr_{0.33}Mn_{1-x}Ti_xO_{3+\delta}$ ($0 \leqslant x \leqslant 0.20$).

the curves corresponding to Mn^{4+} and Mn^{3+} ions and are presented in table 3. Results obtained clearly indicate the presence of greater Mn^{4+} content in the samples compared to a case wherein Ti^{4+} replaces only Mn^{4+} and maintains charge balance. Higher Mn^{4+} content is possible only if substitution of Ti^{4+} is inhomogeneous such that it results in regions of sample that are rich in Mn perhaps surrounded by Ti rich regions.

3.7. XANES

Normalized Mn K-edge XANES spectra of $La_{0.67}Sr_{0.33}Mn_{1-x}Ti_xO_{3+\delta}$ samples, recorded at room temperature, are shown in figure 11. The data were recorded with a step of 1 eV, primarily for EXAFS studies. The main peak arising due to 1s–4p electronic transition and a prepeak at about 15 eV below the main peak are clearly visible in all the spectra. Positions of the main peak and the prepeak are almost the same over the entire doping range ($0.00 \leqslant x \leqslant 0.20$). All peak profiles are very similar to each other. Surprisingly, the chemical shift of the main edge is not observed over the entire doping range. The chemical shift of the inflection point of the main absorption edge is reported to be 4.2 eV for Mn^{3+} and Mn^{4+} ions in $LaMnO_3$ and $CaMnO_3$, respectively [13, 50]. If Ti^{4+} ions substitute Mn^{4+} ions alone, the effective valence of the Mn ion will shift towards 3+ with the increasing doping content x and such a change should be observed in the form of a shift of the main edge in Mn K-edge XANES spectra. Such an effect has been reported in Ti doped $La_{0.7}Ca_{0.3}Mn_{1-x}Ti_xO_3$ samples [51]. The absence of a chemical shift in our sample indicates that the average valence of Mn ions does not change appreciably in our samples, which again supports findings from XPS study.

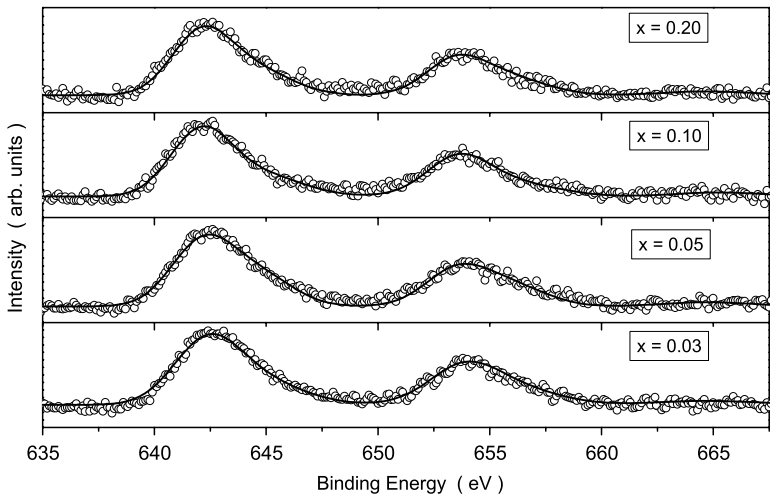

Figure 10. XPS spectra (circles) for low-temperature annealed $La_{0.67}Sr_{0.33}Mn_{1-x}Ti_xO_{3+\delta}$ samples along with the fitted curve (line).

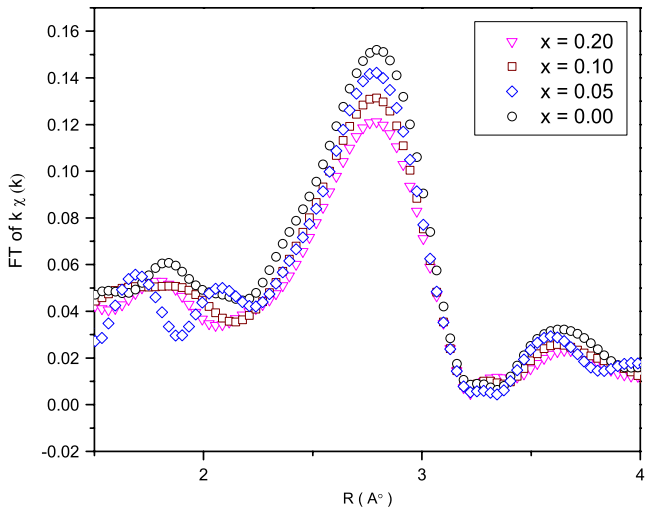

Figure 12. La K-edge Fourier transforms of the low-temperature annealed $La_{0.67}Sr_{0.33}Mn_{1-x}Ti_xO_{3+\delta}$ samples.

Table 4. Structural parameters obtained from La K-edge EXAFS for low-temperature annealed $La_{0.67}Sr_{0.33}Mn_{1-x}Ti_xO_{3+\delta}$ samples. Figures in brackets indicate uncertainties in the last digit.

		$x = 0.00$	$x = 0.05$	$x = 0.10$	$x = 0.20$
La–O_1	R (Å)	2.48(1)	2.43(1)	2.45(1)	2.44(1)
	σ^2 (Å^2)	0.008(2)	0.007(2)	0.006(1)	0.005(1)
	n	3.3(5)	3.3(5)	3.3(3)	3.3(2)
La–O_2	R (Å)	2.64(1)	2.63(1)	2.63(1)	2.62(1)
	σ^2 (Å^2)	0.010(2)	0.008(3)	0.008(1)	0.009(1)
	n	6.2(7)	6.2(6)	6.2(4)	6.2(3)
La–O_3	R (Å)	2.84(2)	2.85(3)	2.86(1)	2.84(1)
	σ^2 (Å^2)	0.005(2)	0.006(3)	0.006(6)	0.009(2)
	n	2.7(6)	2.7(7)	2.7(3)	2.7(5)
La–Mn/Ti	R (Å)	3.39(1)	3.39(1)	3.39(1)	3.39(1)
	σ^2 (Å^2)	0.005(1)	0.005(1)	0.006(1)	0.007(1)
	n	8.1(4)	8.1(4)	8.1(2)	8.1(2)

3.8. EXAFS

EXAFS investigations of the low-temperature annealed samples have been undertaken to see the changes in octahedral environment of Mn due to Ti substitution. Our interest lies mainly in La–(Mn/Ti) and Mn–(Mn/Ti) bond lengths, as these correlations can reveal whether the substitution of Ti^{4+} ions is homogeneous or not. Both La and Mn K-edge EXAFS were fitted initially for the $La_{0.67}Sr_{0.33}MnO_3$ sample. Bond lengths were varied first, followed by their Debye–Waller factors (σ^2). Coordination numbers were initially fixed at the known crystallographic values while fitting Mn K-edge EXAFS, and in case of La K-edge EXAFS 12 La–O bond lengths were divided into three different groups of coordination numbers 3, 6 and 3 respectively on the basis of closeness of their values. Later, coordination numbers had to be varied slightly to improve the quality of fit. The Mn K-edge and La K-edge EXAFS were fitted in tandem so that equal La–Mn bond lengths were obtained from both the EXAFS.

Fourier transforms of La K-edge EXAFS are presented in figure 12. The FT spectra are not corrected for phase shift; however, the values of bond lengths reported in the text and tables are phase corrected values. La K-edge EXAFS were fitted with k-weighting $= 1$, in R-range 1.5–3.5 Å and k-range 3–16 Å^{-1}. Fits of inverse Fourier transforms of La K-edge EXAFS for $x = 0.00, 0.05, 0.10$ and 0.20 samples are presented in figure 13. Results of La K-edge EXAFS analysis are presented in table 4. Nearly constant bond lengths in these materials are in tune with the very similar lattice parameters obtained by analysis of x-ray diffraction spectra of these materials (table 1). As La–(Mn/Ti) correlation in La

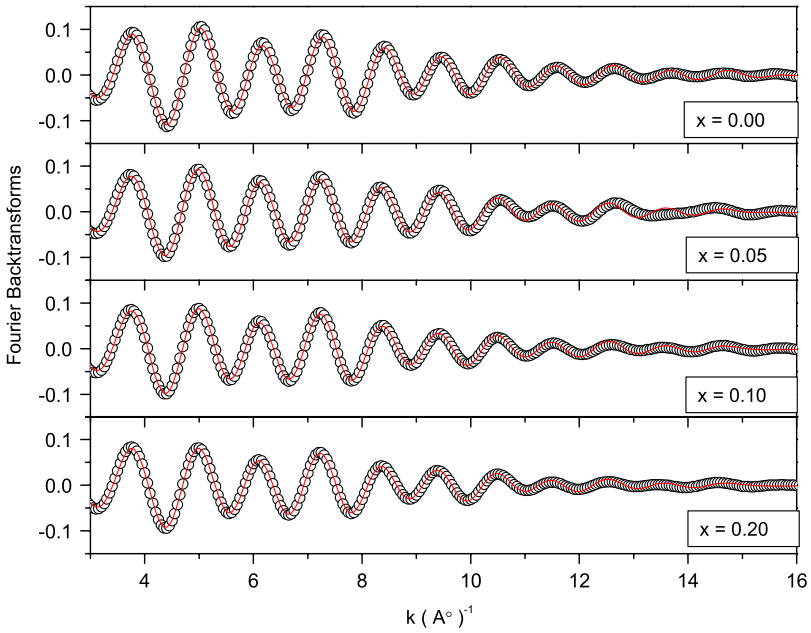

Figure 13. k-weighted backtransformed La K-edge EXAFS spectra (circles) along with fitted curves (line) in $La_{0.67}Sr_{0.33}Mn_{1-x}Ti_xO_{3+\delta}$.

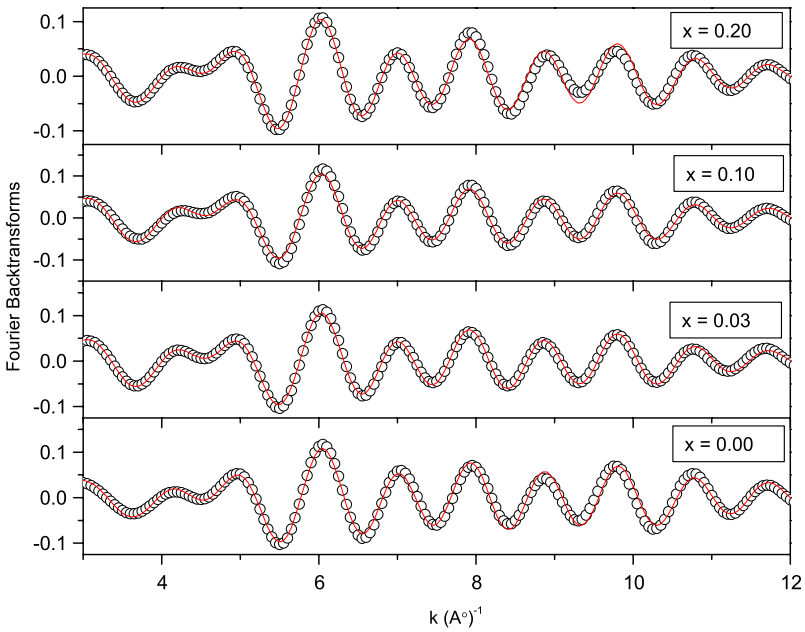

Figure 14. k-weighted backtransformed Mn K-edge EXAFS spectra (circles) along with fitted curves (line) in $La_{0.67}Sr_{0.33}Mn_{1-x}Ti_xO_{3+\delta}$.

K-edge EXAFS includes scattering from $Mn^{3+/4+}$ and Ti^{4+} ions, if Ti^{4+} ions were to selectively replace Mn^{4+} ions the bond length and σ^2 of this correlation should have systematically increased with doping content x. However, no such change is seen in either the bond length or σ^2. Furthermore, the changes in La–O bond lengths and their Debye–Waller factors are small and non-systematic and can be understood in terms of random distribution of Ti^{4+}, Mn^{3+} and Mn^{4+} ions in the sample and resulting oxygen displacement that is permissible in rhombohedral ($R\bar{3}C$) structure. In this structure, the effect of oxygen displacements will be more evident in La–O_1 and La–O_3 bonds compared to La–O_2, which can be seen from the values reported in table 4.

Mn K-edge EXAFS were fitted with k-weighting, in R-range 1–3.6 Å and k-range 3–12 $Å^{-1}$. Fits of the inverse Fourier transforms of Mn K-edge EXAFS for x = 0.00, 0.03, 0.10 and 0.20 are presented in figure 14 and the results of the Mn K-edge analysis are presented in table 5. Mn–O, Mn–Mn as well as Mn–La bond lengths for the samples, obtained by fitting Mn K-edge EXAFS, are almost the same over the entire doping range $0.00 \leqslant x \leqslant 0.20$. Ti substitution should have seriously affected the Mn–O bond length at least at 10% and 20% doping levels due to the ionic size difference. Therefore, a constant bond length could only imply that for most Mn ions the local environment remains unaltered. This is possible only if in the low-temperature annealed samples the Ti substitution is inhomogeneous, leading to creation of Mn rich regions over bulk of the sample separated by Ti rich regions. This is further supported from the fact that the Mn–(Mn/Ti) distance obtained from Mn K-edge EXAFS and the La–Mn distance obtained from Mn K-edge as well as La K-edge EXAFS remains almost the same throughout the series. Therefore, in the case of inhomogeneous doping, even at the high doping level of 20%, the local environment around La and Mn ions would be similar to that in the undoped sample, giving constant bond lengths throughout the series.

Table 5. Structural parameters obtained from Mn K-edge EXAFS for low-temperature annealed $La_{0.67}Sr_{0.33}Mn_{1-x}Ti_xO_{3+\delta}$ samples. Figures in brackets indicate uncertainties in the last digit.

		$x = 0.00$	$x = 0.03$	$x = 0.10$	$x = 0.20$
Mn–O	R (Å)	1.92(0)	1.92(0)	1.92(1)	1.92(1)
	σ^2 ($Å^2$)	0.007(2)	0.007(1)	0.007(2)	0.009(1)
	n	5.5(6)	5.5(3)	5.5(4)	5.7(5)
Mn–(La/Sr)	R (Å)	3.39(1)	3.39(0)	3.39(0)	3.39(0)
	σ^2 ($Å^2$)	0.009(1)	0.010(1)	0.010(1)	0.010(1)
	n	8.4(7)	8.4(5)	8.4(5)	8.6(5)
Mn–(Mn/Ti)	R (Å)	3.81(1)	3.82(0)	3.81(0)	3.82(0)
	σ^2	0.004(1)	0.002(0)	0.003(1)	0.002(1)
	n	5.6(5)	5.6(2)	5.6(2)	5.6(2)
Mn–O–(Mn/Ti)	R (Å)	3.83(1)	3.83(1)	3.83(1)	3.83(1)
	σ^2 ($Å^2$)	0.007(5)	0.007()	0.007(1)	0.007(0)
	n	12.4(6)	12.4(3)	12.4(3)	12.3(4)

4. Discussion

Structural, transport and magnetic properties of Ti doped low-temperature annealed $La_{0.67}Sr_{0.33}MnO_3$ samples have been investigated in the present study. Samples with 10% Ti doping were prepared using two different preparation schedules. The high temperature annealed sample shows transport and magnetic properties similar to those reported in [27] whereas the low temperature annealed sample has significantly different properties. With increasing doping content x, substitution of $Ti^{4+}(3d^0)$ ions in Mn^{4+}–O–Mn^{3+} chains is expected to increase resistivity of the samples. However, low-temperature and high-temperature

annealed $x = 0.10$ samples exhibit significantly different resistivities. Moreover, the high-temperature annealed $x = 0.10$ sample exhibits metal–insulator transition whereas the low-temperature annealed sample is insulating over the entire temperature range investigated. This fact can be understood in terms of additional scattering centers like cation vacancies or substitutional inhomogeneities in the low-temperature annealed sample. The short-range order of the Mn^{4+}–O–Mn^{3+} chain, caused by interspersed Ti ions and cation vacancies, gives rise to the insulating behavior of low-temperature annealed $x \geqslant 0.10$ samples. The strong localizing effect of random cation vacancies is well known [52]. The random potential fluctuations due to cation vacancies and dopant Ti ions favor Anderson type localization, but the localized wave packets are large enough for the e_g electrons to extend over several sites to provide the ferromagnetic interaction. The samples with $x \leqslant 0.05$ exhibit a sharp rise in susceptibility, indicating paramagnetic to ferromagnetic transition, and the ferromagnetic ordering temperature (T_C) decreases with increasing doping content, indicating the gradual weakening of double-exchange coupling. However, for $x = 0.10$ and 0.20 samples, T_C remains at around 300 K, which is significantly higher than those reported for Ti doped manganites [23–25, 27, 29]. The higher T_C of these samples cannot be simply attributed to the presence of cation vacancies. It is to be noted that T_C decreases with increasing cation deficiency in $La_{1-x}Mn_{1-y}O_3$ [53]. In the case of $La_{0.815}Sr_{0.185}MnO_{3+\delta}$ samples, T_C shifts marginally to the higher-temperature side for small δ and shifts towards lower temperatures for higher δ [17]. Hence, high T_C in our low-temperature annealed $x = 0.10$ and $x = 0.20$ samples may not be due to cation vacancies alone; it could be related to Ti doping as well. Moreover, susceptibility (emu/f.u.) of these $x = 0.10$ and 0.20 samples is significantly smaller and cannot be explained only on the basis of substitution of Mn^{4+} ions by non-magnetic Ti^{4+} ($3d^0$) ions. A decrease in susceptibility of such a magnitude is not observed in Ti doped samples of the same composition [26, 27, 29]. T_C of our high-temperature annealed $x = 0.10$ sample matches closely with the reported value of T_C [27]. In fact, susceptibility is found to be higher in cation deficient samples than that in stoichiometric samples [54] and have similar magnitudes in [17]. Reduced susceptibility in our low-temperature annealed samples can be explained to be due to the formation of isolated Mn rich regions where DE is active and separated by Ti rich regions. These regions are created due to inhomogeneous Ti substitution.

IR spectra indicate that Ti is predominantly in tetravalent state in these compounds. Moreover, IR spectra exhibit a slight shift in the stretching mode absorption peak in our samples. It has been argued on the basis of fixed Mn–O stretching mode absorption peaks in $La_{0.67}Ca_{0.33}Mn_{1-x}Ti_xO_3$ that Jahn–Teller distortions are not affected by doping of Ti ions in the materials [23]. In the case of low-temperature annealed samples, the 600 cm^{-1} mode is rather broadened. This can be related to the presence of disorder in the Ti doping. In this sample Ti^{4+} substitution causes regions wherein double-exchange is active and regions which are devoid of double-exchange pairs. Perhaps the two regions are in such a proportion that the strengths of respective stretching modes are nearly the same, resulting in a broad absorption dip. XRD studies indicate the complete solid solubility of Ti in the parent $R\bar{3}C$ structure of $La_{0.67}Sr_{0.33}MnO_3$ with lattice parameters of the low-temperature annealed samples remaining nearly the same over the entire doping range. This also supports the above idea of inhomogeneous substitution of Ti^{4+} ions. Such a substitution would result in formation of Mn rich regions that are isolated from each other by regions that are rich in Ti. This would increase the magnitude of resistivity due to additional scattering from the Ti rich regions, inhibit insulator to metal transition and suppress magnetic order as well as magnetoresistance, all of which are seen in low-temperature annealed $x = 0.1$ and 0.2 samples. The weak ferromagnetic transition seen in these two samples at about 300 K could then be explained to be due to ordering of Mn rich regions connected with each other by a variable range hopping polaron. The VRH of charge carriers strengthens ferromagnetic exchange coupling between isolated ferromagnetic regions and manifests in a weak ferromagnetic-like transition at room temperature.

EXAFS results provide further evidence for the inhomogeneous substitution of Ti ions. Local structure around La and Mn ions is found to be almost the same in doped as well as the undoped samples (table 4, 5). This indicates that even at 20% dopant concentration large parts of the sample have Mn ions in exactly the same environment as in the undoped sample. In the low-temperature annealed $x = 0.10$ sample, Mn^{4+} and Mn^{3+} contents are found to be nearly 28% and 62% respectively (table 3). If the substitution was homogeneous, 10% Ti ions would have depleted the Mn^{4+} concentration so as to maintain charge balance. Instead, in the low-temperature annealed samples, it can be seen that Mn^{4+} concentration decreases at a much slower rate, indicating the presence of isolated Mn rich regions.

5. Conclusions

In this paper studies of structural, magnetic, transport and spectroscopic properties of low-temperature annealed $La_{0.67}Sr_{0.33}Mn_{1-x}Ti_xO_3$ ($0 \leqslant x \leqslant 0.20$) are presented. The lower annealing temperature results in an inhomogeneous substitution of Ti ions resulting in a very similar crystal structure and local structure around La and Mn ions but vastly different magnetic and transport properties as compared to the undoped sample. This is perhaps due to the formation of isolated ferromagnetic clusters linked to each other by a variable range hopping polaron.

Acknowledgments

K R Priolkar acknowledges financial assistance from DST under SR/FTP/PS-19/2003. Thanks are also due to Professor M S Hegde, Indian Institute of Science, Bangalore, for useful discussions and constant encouragement, and to Dr N Y Vasanthacharya for DC susceptibility measurements. XAFS measurements were performed at SPring-8 under proposal **2003A0028-Cx-np** with financial assistance for travel from DST, New Delhi.

References

[1] Tokura Y (ed) 2000 *Colossal Magnetorestive Oxides* (New York: Gordon and Breach Science)
[2] Rao C N R and Raveau B (ed) 1998 *Colossal Magnetoresistance, Charge Ordering and Related Properties of Manganese Oxides* (Singapore: World Scientific)
[3] Tofield B C and Scott W R 1974 *J. Solid State Chem.* **10** 183
[4] Sakai N, Fjellvåg H, Lebech B and Fernandez-Diaz M T 1997 *Acta Chem. Scand.* **51** 904
[5] Maignan A, Michel C, Hervieu M and Raveau B 1997 *Solid State Commun.* **104** 277
[6] Geller S 1956 *J. Chem. Phys.* **24** 1236
[7] van Roosmalen J A M, Cordfunke E H P, Helmholdt R B and Zandgergen H W 1994 *J. Solid State Chem.* **110** 100
[8] Mizusaki J, Yonemura Y, Kamata H, Ohyama K, Mori N, Takai H, Tagawa H, Dokiya M, Naraya K, Sasamoto T, Inaba H and Hashimoto T 2000 *Solid State Ion.* **132** 167
[9] Maguire E T, Coats A M, Skakle J M S and West A R 1999 *J. Mater. Chem.* **9** 1337
[10] Hervieu M, Mahesh R, Rangavittal N and Rao C N R 1995 *Eur. J. Solid State Inorg. Chem.* **32** 79
[11] van Roosmalen J A M and Cordfunke E J P 1994 *J. Solid State Chem.* **110** 106
[12] Ferris V, Brohan L, Ganne M and Tournoux M 1995 *Eur. J. Solid State Inorg. Chem.* **32** 131
[13] Dezanneau D, Audier M, Vincent H, Meneghini C and Djurado E 2004 *Phys. Rev.* B **69** 014412
[14] Trukhanov S V, Bushinsky M V, Troyanchuk I O and Szymczak H 2004 *J. Exp. Theor. Phys.* **99** 756
[15] Trukhanov S V, Lobanovski L V, Bushinsky M V, Khomchenko M A, Pushkarev N V, Troyanchuk I O, Maignan A, Flahaut D, Szymczak H and Szymczak R 2004 *Eur. Phys. J.* B **42** 51
[16] Dabrowski B, Rogacki K, Xiong X, Klamut P W, Dybzinski R, Shaffer J and Jorgensen J D 1998 *Phys. Rev.* B **58** 2716
[17] Bukowski Z, Dabrowski B, Mais J, Klamut P W, Kolesnik S and Chmaissem O 2000 *J. Appl. Phys.* **87** 5031
[18] Mitchell J F, Argyriou D N, Potter C D, Hinks D G, Jorgensen J D and Bader S D 1996 *Phys. Rev.* B **54** 6172
[19] Mizusaki J, Mori N, Takai H, Yonemura Y, Minamiue H, Tagawa H, Dokiya M, Inaba H, Naraya K, Sasamoto T and Hashimoto T 2000 *Solid State Ion.* **129** 163
[20] Roosmalen J A M, van Vlaaderen P, Cordfunke E H P, Ijdo W L and Ijdo D J W 1995 *J. Solid State Chem.* **114** 516
[21] Toepfer J and Goodenough J B 1997 *Solid State Ion.* **101–103** 1215
[22] Nakamura K 2003 *J. Solid State Chem.* **173** 299
[23] Liu X, Xu X and Zhang Y 2000 *Phys. Rev.* B **62** 15112
[24] Sahana M, Venimadhav A, Hegde M S, Nenkov K, Roßler U K, Dorr K and Muller K-H 2003 *J. Magn. Magn. Mater.* **260** 361
[25] Hu J, Qin H, Chen J and Wang Z 2002 *Mater. Sci. Eng.* B **90** 146
[26] Troyanchuk I O, Bushinsky M V, Szymczak H, Barner H and Maignan A 2002 *Eur. J. Biochem.* **28** 75
[27] Kallel N, Dezanneau G, Dhahri J, Oumezzine M and Vincent H 2003 *J. Magn. Magn. Mater.* **261** 56
[28] Liu Y-H, Huang B-X, Zhang R-Z, Yuan X-B, Wang C-J and Mei L-M 2004 *J. Magn. Magn. Mater.* **269** 398
[29] Kim M S, Yang J B, Cai J, Zhou X D, James W J, Yelon W B, Parris P E, Buddhikot D and Malik S K 2005 *Phys. Rev.* B **71** 014433
[30] Ulyanov A N, Kang Y-M, Yoo S-I, Yang D-S, Park H M, Lee K-W and Yu S-C 2006 *J. Magn. Magn. Mater.* **304** e331
[31] Ulyanov A N, Yang D-S, Lee K-W, Greneche J-M, Chau N and Yu S-C 2006 *J. Magn. Magn. Mater.* **300** 175
[32] Alvarez-Serrano I, Lopez M L, Pico C and Viega M L 2006 *Solid State Sci.* **8** 37
[33] Nam D N H, Bau L V, Khiem N V, Dai N V, Hong L V, Phuc N X, Newrock R S and Nordblad P 2006 *Phys. Rev.* B **73** 184430
[34] Zhu X B, Sun Y P, Ang R, Zhao B C and Song W H 2006 *J. Phys. D: Appl. Phys.* **39** 625
[35] Priolkar K R and Rawat R 2008 *J. Magn. Magn. Mater.* **320** 325
[36] Bajpai A and Bannerjee A 1997 *Rev. Sci. Instrum.* **68** 4075
[37] Newville M, Livins P, Yacoby Y, Rehr J J and Stern E A 1993 *Phys. Rev.* B **47** 14126
[38] Rehr J J, Albers R C and Zabinsky S I 1992 *Phys. Rev. Lett.* **69** 3397
[39] Popovič Z V, Cantarero A, Thijssen W H A, Paunovič N, Dohcevič-Mitrovič N and Sapina F 2005 *J. Phys.: Condens. Matter* **17** 351
[40] De Marzi G, Popovič Z V, Cantarero A, Dohcevič-Mitrovič Z, Paunovič N, Bok J and Sapina F 2003 *Phys. Rev.* B **68** 064302
[41] Mahendiran R, Tiwary S K, Raychoudhuri A K, Ramadrishnan T V, Mahesh R, Rangavittal N and Rao C N R 1996 *Phys. Rev.* B **53** 3348
[42] Blasco J, Garcia J, Teresa J M, Ibarra M R, Perez J, Algarabel P A, Marquina C and Ritter C 1997 *Phys. Rev.* B **55** 8905
[43] Sundaresan A, Paulose P L, Mallik R and Sampathkumaran E V 1998 *Phys. Rev.* B **57** 2690
[44] Zhu H, Liu X, Ruan K and Zhang Y 2002 *Phys. Rev.* B **65** 104424
[45] Hébert S, Wang B, Maignan A, Martin C, Retoux R and Raveau B 2002 *Solid State Commun.* **123** 311
[46] Kusters R M, Singleton D A, Keen D A, McGreevy R and Hayes W 1989 *Physica* B **155** 362
[47] Snyder G J, Hiskes R, DiCarolis S, Beasley M R and Geballe T H 1996 *Phys. Rev.* B **53** 14434
[48] Viret M, Ranno L and Coey J M D 1997 *Phys. Rev.* B **55** 8067
[49] Hwang H, Cheong S-W, Ong N P and Batlogg B 1996 *Phys. Rev. Lett.* **77** 2041
[50] Subías G, García J, Proietti M G and Blasco J 1997 *Phys. Rev.* B **56** 8183
[51] Cao D 2001 *Phys. Rev.* B **64** 184409
[52] Coey J M D, Viret M, Ranno L and Ounadjela K 1995 *Phys. Rev. Lett.* **75** 3910
[53] de Silva P S I P N, Richards F M, Cohen L F, Alonso J A, Martinez-Lope M J, Casais M T, Thomas K A and MacManus-Driscoll J L 1998 *J. Appl. Phys.* **83** 395
[54] Ranno I, Viret M, Mari A, Thomas R M and Coey J M D 1996 *J. Phys.: Condens. Matter* **8** L33